International Journal of Heat and Mass Transfer 52 (2009) 3000–3008

Contents lists available at ScienceDirect

International Journal of Heat and Mass Transfer

journal homepage: www.elsevier.com/locate/ijhmt

Growth and detachment of carbon dioxide bubbles on a horizontal porous surface with a uniform mass injection

Shong-Leih Lee *, Wen-Bin Tien

Department of Power Mechanical Engineering, National Tsing Hua University, Hsinchu 30013, Taiwan

ARTICLE INFO

Article history:
Received 26 December 2007
Received in revised form 9 December 2008
Accepted 21 January 2009
Available online 26 March 2009

Keywords:
Bubble growth
Bubble detachment
Uniform mass injection
Contact angle

ABSTRACT

Growth and detachment of carbon dioxide bubbles on a horizontal porous surface in water is investigated in this paper. Uniform carbon dioxide injection on the porous surface is considered. The Young–Laplace equation is solved with the geometry method to yield the bubble shape. The dynamic pressure on the bubble surface due to bubble expansion is neglected. Multi-solution modes are found. Based on the characteristics of the solution modes, it is postulated that the bubble grows with a monotonically increasing base area until the maximum value is reached according to the fundamental solution mode. After that, the bubble jumps toward the secondary solution mode at a constant volume, and then detaches from the surface. The increasing rate of the bubble volume due to mass diffusion/convection is evaluated by solving the momentum and concentration equations. Evolution of the bubble shape then is determined corresponding to the variation of the bubble volume. The numerical results indicate that hydrophobic surface produces large bubble and thus gives rise to better efficiency for dissolved gas removal.

1. Introduction

Growth and detachment of bubbles has been the subject of many investigations in the past decades. The flow configurations examined in the previous studies include at least gas injection through a thin wall tube (or an orifice on a flat plate) submerged in liquid [1–6], boiling on a heated surface [7–10], and bubble growth in solutions supersaturated with a gas [11–14]. Many of the conventional studies treated the bubble as a whole or truncated sphere [2,7,8,11–14]. However, the existing experimental observations [3–6,10] revealed that the bubble is generally not spherical due to the presences of gravity force (large Bond number), contact angle, surface geometry, bubble dynamics (inertia and viscosity), etc. especially when the status of the bubble is near detachment.

There are a few numerical methods for the shapes of axisymmetric nonspherical bubbles. Among them, Pitts [15] and Sonoyama and Iguchi [3] determined the bubble shape by minimizing the total free energy of a bubble at a given volume. Chesters [16,17] solved the Young–Laplace equation with a perturbation approach in cylindrical coordinates (z,r). The bubble shape was represented with the function $z = z(r)$ to circumvent the singularity $df/dz = \infty$ at the bubble tip ($r = 0$) if the function $r = f(z)$ was employed instead. However, the function $z = z(r)$ poses to the singularity $dz/dr = \infty$ too when the bubble is necking. Oguz and Prosperetti [1] solved the Young–Laplace equation with the boundary integral method to obtain the shape evolution of a bubble that grew and detached from a submerged small thin wall tube. Two different growth regimes were found to exist according to whether the gas flow rate into the bubble was smaller or greater than a critical value. Recently, Chen and Groll [9] solved the Young–Laplace equation in arc-length coordinates (i.e. $r = r(s)$, $z = z(s)$) by using the Runge–Kutta method of order four. A few parameters appearing in the numerical formulation were determined such that the real bubble shape (from experiment) was best fitted.

Another point of controversy has been the matter of bubble detachment. Bubble detachment is a natural consequence of the dynamics of bubble growth. Due to the lack of reliable information, the bubble is generally forced to detach when some criterion has been satisfied. However, there is still no consistency on the definition of bubble detachment criterion. Force balance of an attached bubble as a whole has been widely employed for the definition of bubble detachment criterion [2,7,9,12,13,18,19]. The forces considered in this branch of bubble detachment criteria include buoyancy force, pressure force on the contact area, surface tension force, drag force, inertial force, etc. The contact angle is another popular indicator for bubble detachment criterion. In this branch, bubble detachment is judged to occur when the contact angle reaches a critical value, e.g. 70° in Duhar and Colin [4,5], 90° in Bisperink and Prins [11], and 5–35° in Uzel et al. [14]. Some other criteria for bubble detachment include (a) the bubble volume reaches the maximum possible value [15–17], (b) the neck diameter of the bubble is smaller than one micrometer [6] or smaller than 10% of

* Corresponding author. Tel.: +886 35728230; fax: +886 35722840.
E-mail address: sllee@pme.nthu.edu.tw (S.-L. Lee).

0017-9310/$ - see front matter © 2009 Elsevier Ltd. All rights reserved.
doi:10.1016/j.ijheatmasstransfer.2009.01.040

the tube diameter [1], (c) the contact area rapidly decreases to zero [8], and (d) minimization of Lagrange function is judged to have no reasonable solution [3].

The direct methanol fuel cell (DMFC) has attracted much attention due to its potential applications as a power source for transportation and portable electronic devices. On the anode side of a DMFC, carbon dioxide is produced as a result of methanol electrochemical oxidation. The produced carbon dioxide (dissolved in water) diffuses through a back layer and forms bubbles on the outer surface of the back layer [20]. The carbon dioxide bubble should be removed efficiently. Otherwise, the anode channels will be blocked, leading to limited mass transport. In the present study, the back layer (usually made of carbon cloth or carbon paper) is regarded as a porous medium. Growth and detachment of carbon dioxide bubbles on the porous surface will be investigated with a proposed bubble detachment criterion.

2. Theoretical analysis

2.1. Governing equations

Consider a water of semi-infinity ($Z \geqslant \infty$) above an infinite horizontal porous surface on the XY-plane. Initially, the water is pure and stationary. At $t > 0$, a uniform carbon dioxide flux Q injects from the porous surface such that carbon dioxide bubbles nucleate, grow, and detach at some particular sites on the porous surface. The static contact angle of carbon dioxide bubble on carbon cloth in water is approximately $\theta = 65°$. The bubble growth due to mass diffusion is very slow in the present case. Hence, the contact angle is assumed to remain as $\theta = 65°$ throughout the whole bubble growth period [21] for simplicity. The process is isothermal and incompressible. Evaporation of water is neglected. Bubbles nucleate only on the porous surface. Any two neighboring nucleation sites have the same distance such that the problem can be formulated for a single site inside a hexangular cylinder. For simplicity, the physical domain is further simplified as an axisymmetric problem inside a circular cylinder of radius R_0. The configuration of the problem is depicted in Fig. 1 in a dimensionless cylindrical coordinates (z,r) normalized with a reference length L, i.e.

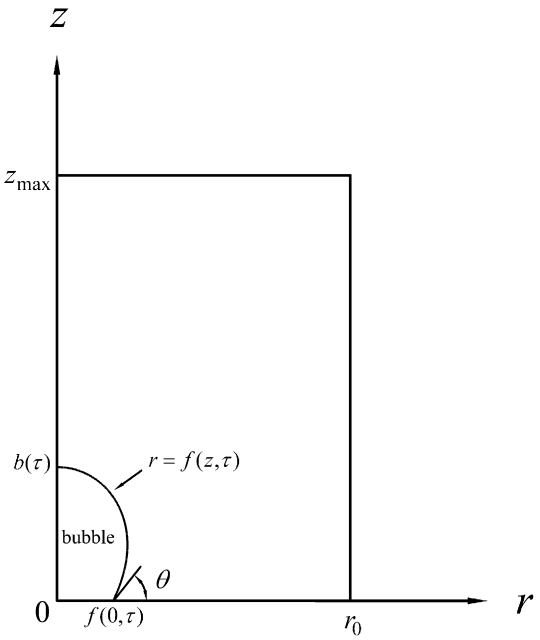

Fig. 1. Flow configuration and coordinate system of the problem.

$$z = Z/L, \quad r = R/L, \quad r_0 = R_0/L \tag{1}$$

The bubble shape is represented by

$$r = f(z,\tau) \tag{2}$$

where

$$f(z,\tau) = F(Z,t)/L, \quad \tau = t/t_c \tag{3}$$

The reference length L and reference time t_c are to be defined. The bubble has a height $b(\tau)$, a base radius $f(0,\tau)$, and a contact angle θ. The natural convection effect is neglected. All of the thermophysical properties are assumed constant.

After imposing the above assumptions and making the following dimensionless transformation

$$u = U/U_c, \quad v = V/U_c, \quad t_c = L/U_c, \quad \rho^* = \frac{\rho}{\rho_l}, \quad \mu^* = \frac{\mu}{\mu_l},$$
$$p = \frac{P - P_{ref}}{\rho_l U_c^2}$$
$$Re_c = \frac{\rho_l U_c L}{\mu_l}, \quad Fr_c = \frac{U_c}{\sqrt{gL}}, \quad Pe_c = \frac{U_c L}{D_l}, \quad \phi = C/C_{ref}$$
$$\hat{p} = \begin{cases} Re_c\left(p + Fr_c^{-2}(z - z_{ref})\right) + c_1 & \text{in liquid} \\ Re_c\left(p + \frac{\rho_g}{\rho_l} Fr_c^{-2}(z - z_{ref})\right) + c_2 & \text{in gas} \end{cases} \tag{4}$$

the governing equations can be written as

$$\frac{\partial(ru)}{\partial z} + \frac{\partial(rv)}{\partial r} = 0 \tag{5}$$

$$\rho^* Re_c\left(\frac{\partial u}{\partial \tau} + u\frac{\partial u}{\partial z} + v\frac{\partial u}{\partial r}\right) = \frac{\partial \hat{p}}{\partial z} + \frac{1}{r}\left[\frac{\partial}{\partial z}\left(\mu^* r\frac{\partial u}{\partial z}\right) + \frac{\partial}{\partial r}\left(\mu^* r\frac{\partial u}{\partial r}\right)\right] \tag{6}$$

$$\rho^* Re_c\left(\frac{\partial v}{\partial \tau} + u\frac{\partial v}{\partial z} + v\frac{\partial v}{\partial r}\right) = -\frac{\partial \hat{p}}{\partial r} + \frac{1}{r}\left[\frac{\partial}{\partial z}\left(\mu^* r\frac{\partial v}{\partial z}\right) + \frac{\partial}{\partial r}\left(\mu^* r\frac{\partial v}{\partial r}\right)\right] - \mu^*\frac{v}{r^2} \tag{7}$$

$$Pe_c\left(\frac{\partial \phi}{\partial \tau} + u\frac{\partial \phi}{\partial z} + v\frac{\partial \phi}{\partial r}\right) = \frac{1}{r}\left[\frac{\partial}{\partial z}\left(r\frac{\partial \phi}{\partial z}\right) + \frac{\partial}{\partial r}\left(r\frac{\partial \phi}{\partial r}\right)\right] \tag{8}$$

where (u,v) is the velocity in the cylindrical coordinate system (z,r). The reference quantities including velocity U_c, pressure P_{ref}, concentration C_{ref}, and altitude z_{ref} are to be determined. Mathematically, the dimensionless density ρ^* and viscosity μ^* are step functions across the bubble surface. They have the value of unity in the liquid region and jump to another constant in the gas region, i.e.

$$\rho^* = \begin{cases} 1 & \text{in liquid} \\ \rho_g/\rho_l & \text{in gas} \end{cases} \tag{9a}$$

$$\mu^* = \begin{cases} 1 & \text{in liquid} \\ \mu_g/\mu_l & \text{in gas} \end{cases} \tag{9b}$$

where the subscripts g and l denote, respectively, the properties of the gas and the liquid. Note also that the concentration Eq. (8) applies only in the liquid region. Inside the bubble, the perfect-gas law

$$P_g = \rho_g \Re T \tag{10}$$

is used instead, where $\Re$ and T are the gas constant and temperature, respectively.

2.2. Bubble shape

Across the bubble surface, the pressure jump is expressible as the Young–Laplace equation [22,23]

$$p_l - p_g = \frac{1}{Re_c}\left(\frac{-\kappa}{Ca_c} + (\sigma_{nn})_l - \left(\frac{\mu_a}{\mu_l}\right)(\sigma_{nn})_a\right) \tag{11a}$$

$$Ca_c = \frac{\mu_l U_c}{\gamma}, \quad \sigma_{nn} = 2\frac{\partial v_n}{\partial n} \tag{11b}$$

where γ is the surface tension, and Ca_c is the characteristic capillary number. The dimensionless curvature of the free surface κ (has been normalized by L^{-1}) is positive for a concave liquid surface. It can be evaluated from the principal curvatures κ_1 and κ_2, i.e.

$$\kappa = \kappa_1 + \kappa_2 \tag{12a}$$

$$\kappa_1 = \frac{-f''}{(1+f'^2)^{1.5}} \tag{12b}$$

$$\kappa_2 = \frac{1}{f(1+f'^2)^{0.5}} \tag{12c}$$

where $r = f(z,\tau)$ represents the bubble shape as defined in Eq. (2). The primes stand for the partial differentiation with respect to z. In the present problem, the bubble is assumed to grow gradually such that the normal stress σ_{nn} on the bubble surface is negligible. Hence, the Young–Laplace Eq. (11a) reduces to

$$\begin{aligned} &\hat{p}_l - \hat{p}_a = \Delta\hat{p} = \frac{1}{Ca_c}\left(Bo(z - z_{ref}) - \kappa\right) + \text{constant} \\ &\kappa = Bo\ z - \left(Bo\ z_{ref} + Ca_c(\Delta\hat{p} - \text{constant})\right) \end{aligned} \tag{13}$$

where the constant comes from the arbitrary constants c_1 and c_2 in Eq. (4). The Bond number is defined as

$$Bo = \frac{(\rho_l - \rho_g)g\ L^2}{\gamma} \tag{14}$$

which represents the hydrostatic buoyancy force.

It is important to note that the quantity $\hat{p}$ appearing in the momentum Eqs. (6) and (7) is a flow-induced pressure (known as dynamic pressure [9]). In quiescent fluids, the pressure $\hat{p}$ has a zero gradient in all directions and thus becomes an arbitrary constant in each fluid. This means that the pressure jump $\Delta\hat{p}$ can be treated as an arbitrary constant. In the present study, the flow due to bubble growth is assumed very weak such that variation of the pressure jump $\Delta\hat{p}$ along the bubble surface is negligibly small as compared to the hydrostatic buoyancy force. Therefore, the Young–Laplace Eq. (13) further reduces to

$$\kappa = \kappa_{tip} + (z - b) \tag{15}$$

if the reference length is assigned as

$$L = \sqrt{\frac{\gamma}{(\rho_l - \rho_g)g}} \tag{16}$$

to yield $Bo = 1$, where κ_{tip} is the curvature of the bubble tip at $z = b$. Eq. (15) indicates that the curvature decreases linearly from $\kappa = \kappa_{tip}$ at the bubble tip ($z = b$) to $\kappa = \kappa_{tip} - b$ at the bubble base ($z = 0$) due to the hydraulic buoyancy force. The value of z_{ref} has been absorbed into κ_{tip} and thus does not affect the formulation (15).

Eqs. (12) and (19) form a nonlinear second-order ordinary differential equation for the bubble shape $r = f(z,\tau)$. The associated boundary conditions are

$$f(b,\tau) = 0, \quad f'(b,\tau) = -\infty, \quad f'(0,\tau) = -cot\theta \tag{17}$$

The problem is time-dependent because the bubble height b depends on time. It is of great numerical difficulty to solve the problem due to the fact that $f(z,\tau)$ has an infinite derivative at the bubble tip. Numerical difficulty would arise also from the Neumann boundary condition at the bubble base when the contact angle is zero ($\theta = 0$). In the present study, the problem is solved with the geometry method [23] that handles the evolute of a curve (center of curvature) rather than the curve itself. Such a strategy circumvents the numerical difficulty successfully.

For a given bubble height b and a tip curvature κ_{tip}, the bubble shape can be obtained by solving Eqs. (12), (15) and (17). Fig. 2(a) shows the resulting contact angle θ on the porous surface ($z = 0$) as a function of κ_{tip} under a few prescribed bubble heights b. From Fig. 2(a) it is found that the problem could have multiple solutions for a given b. For instance, there are at least three solution modes for the case of $b = 1.4$ that satisfy all of the boundary conditions (17) with $\theta = 65°$. As depicted in Fig. 2(b), the three solution modes share the same bubble height and contact angle, although their tip

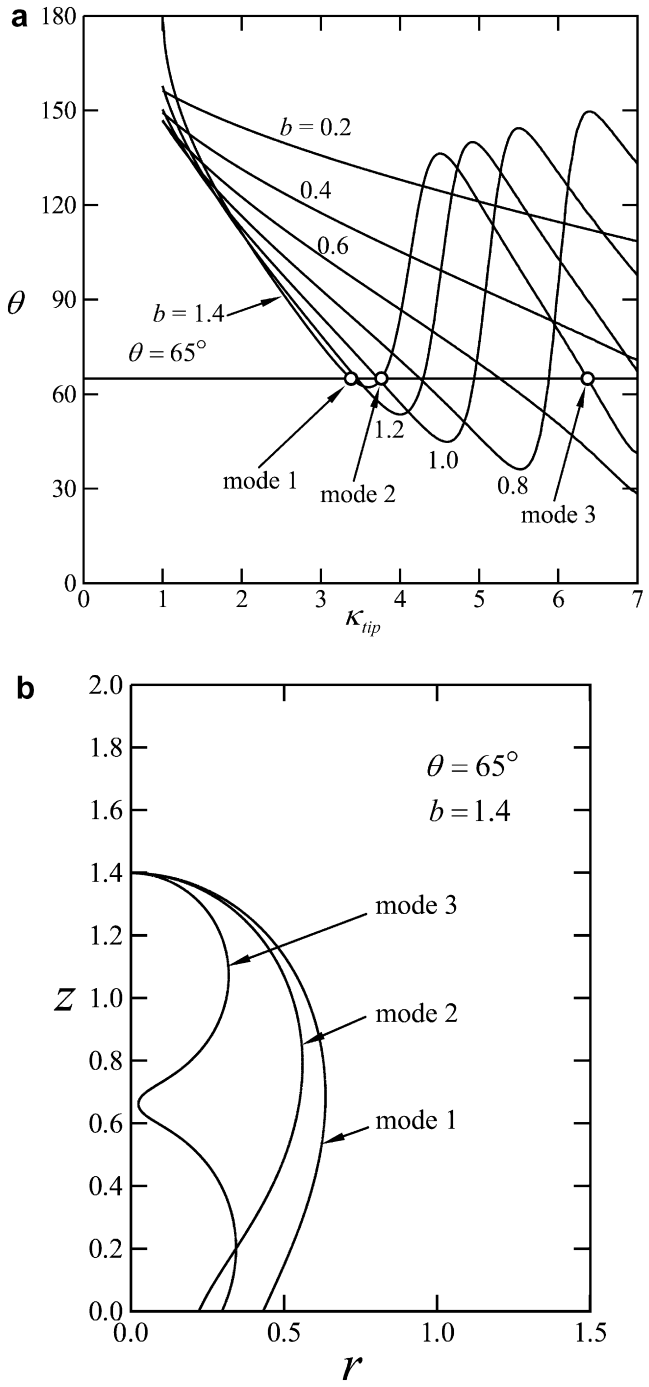

Fig. 2. (a) The resulting contact angle θ as a function of κ_{tip} at various b. (b) The three solution modes at $\theta = 65°$ and $b = 1.4$.

curvatures κ_{tip} are different. For convenience, the bubble volume is evaluated from

$$v(b) = \int_0^b f^2(z)dz \tag{18}$$

which has been normalized by πL^3. The resulting bubble volume as a function of b is shown in Fig. 3 for each of the three solution modes. As expected, mode 1 always has a bubble volume larger than that of mode 2 at the same bubble height (see Fig. 2(b)). In the course of increasing b from 1.40 to 1.50, solution modes 1 and 2 approach each other and eventually coincide and then both disappear at $b > 1.46$.

2.3. Bubble detachment

Recently, Nam et al. [10] found that the ebullition cycle of bubble detachment could be divided into two periods. In the growth period the residual bubble nucleus grew until its base area reached the maximum value. The detachment period included base area shrinking, bubble neck forming, and bubble detaching from the wafer surface. The detachment period in their experiment lasted only 0.15 s as compared to 1.60 s in the growth period. This implies that the bubble volume is essentially constant in the whole detachment period because the duration time is very short as remarked by Uzel et al. [14].

Among the many possible equilibrium shapes of the bubble, only solution mode 1 could occur naturally. Fig. 4(a) shows the volume v, the base area $f^2(0)$, and the tip curvature κ_{tip} as functions of b for solution mode 1 subject to the contact angle $\theta = 65°$. The bubble shapes for various bubble heights are plotted in Fig. 4(b), where the cases $b = 1.15$ and $b = 1.40$ possess the maximum base area and the maximum volume, respectively. For convenience, the volume to base area ratio $v/f^2(0)$ versus the volume is presented in Fig. 4(c). The bubble becomes less stable when the volume to base area ratio increases. Hence, the parameter $v/f^2(0)$ could be a good measure for stability of equilibrium bubbles. Theoretically, when bubble grows (or bubble volume increases) both bubble height b and base area increase monotonically until the maximum base area is reached at $v = 0.3241$ (see Fig. 4(a)). In the course of bubble growth, the volume to base area ratio $v/f^2(0)$ increases linearly in the range of $0.08 \leqslant v \leqslant 0.32$ as observable from Fig. 4(c). After that, $v/f^2(0)$ has a sharp increase. Beyond the maximum volume, equilibrium bubble does not seem possible. Hence, the maximum volume can be regarded as the upper limit of equilibrium bubbles [15–17].

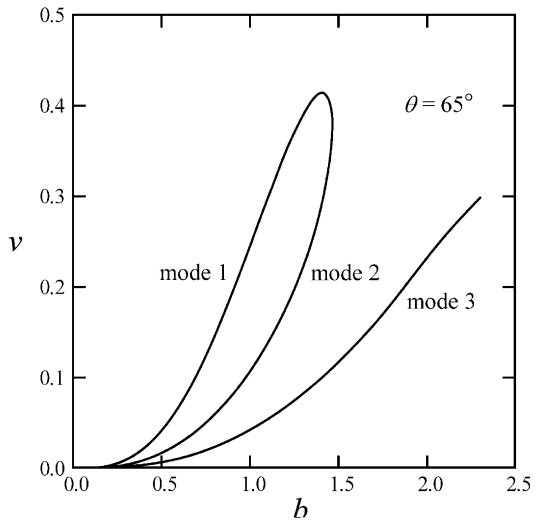

Fig. 3. Bubble volume as a function of b for different solution modes.

Due to hydraulic instability, however, bubble detachment might occur somewhere in the region $0.3241 \leqslant v \leqslant 0.4135$, i.e. the interval between the two white dots in Fig. 4(c). For convenience, this particular range of bubble volume will be referred to as "critical equilibrium bubbles".

Fig. 3 reveals that solution modes 1 and 2 form a single close loop. This means that the Young–Laplace equation has at least two solutions for a given volume below the maximum volume. Among the solutions, the one having the lowest bubble height is redefined as solution mode 1 for convenience, while solution mode 2 has the second lowest height. Solution mode 3 is defined similarly if exists. It is important to note that solution mode 2 always possesses a "neck" because it is taller than solution mode 1 under the same volume.

As mentioned earlier, the bubble volume is essentially constant in the detachment period. In the present study, bubble detachment is assumed to occur at the lower limit of the "critical equilibrium bubbles" in view of possible perturbation from the environment. Therefore, it is postulated that in the growth period the bubble grows with a monotonically increasing base area until the maximum value is reached according to solution mode 1. After that, the bubble jumps toward solution mode 2 at a constant volume, and then detaches from the surface. Transition between the two solution modes can be attributed to hydraulic instability. Fig. 5 shows the bubble shapes of solution modes 1 and 2 at the same volume $v = 0.3241$ for the case of $\theta = 65°$. The height and base area $(b, f^2(0))$ of the two bubbles are $(1.15, 0.2440)$ and $(1.43, 0.06876)$. This means that the bubble should experience a very severe base area shrinking (the base area ratio is 0.2828) when jumps from solution mode 1 toward solution mode 2 in the detachment period. Although experimental evidence for the jumping from solution modes 1 to 2 is lacking, the postulation has no influence on the problem before bubble detachment.

2.4. Boundary conditions

For simplicity, the governing Eqs. (5)–(8) are solved only in the liquid region in the present study. Hence, both ρ^* and μ^* are assigned as unity in the momentum Eqs. (6) and (7). This implies the need of a set of properly defined boundary conditions on the bubble surface. On the liquid side of the bubble surface, the saturation concentration is

$$C_s = \frac{P_l}{H} = \frac{P_g - \gamma\kappa/L}{H} \tag{19}$$

based on the Henry law and the Young–Laplace Eq. (11a), where H is the Henry constant [24]. This leads to the boundary condition

$$\phi(z, f, \tau) = 1 - \Omega\kappa = 1 - \Omega(\kappa_{tip} + z - b) \tag{20a}$$

$$\Omega = \frac{\gamma}{P_g L} \tag{20b}$$

for the concentration Eq. (8) on the bubble surface if the reference concentration is assigned as

$$C_{ref} = \frac{P_g}{H} \tag{21}$$

When the concentration $\phi(z, r, \tau)$ in the liquid region is available, the mass increasing rate inside the bubble at time τ can be evaluated from

$$Pe_c \Theta \frac{dv(\tau)}{d\tau} = qf^2(0, \tau) + 2\int_\Gamma f(z, \tau)\left(\frac{\partial\phi}{\partial r}dz + \frac{\partial\phi}{\partial z}dr\right) \tag{22a}$$

$$\Theta = \frac{\rho_g}{C_{ref}}, \quad q = \frac{Q}{Q_c}, \quad Q_c = \frac{D_l C_{ref}}{L} \tag{22b}$$

where Γ denotes the bubble surface while the second term on the RHS of Eq. (22a) denotes the net mass influx from the liquid region

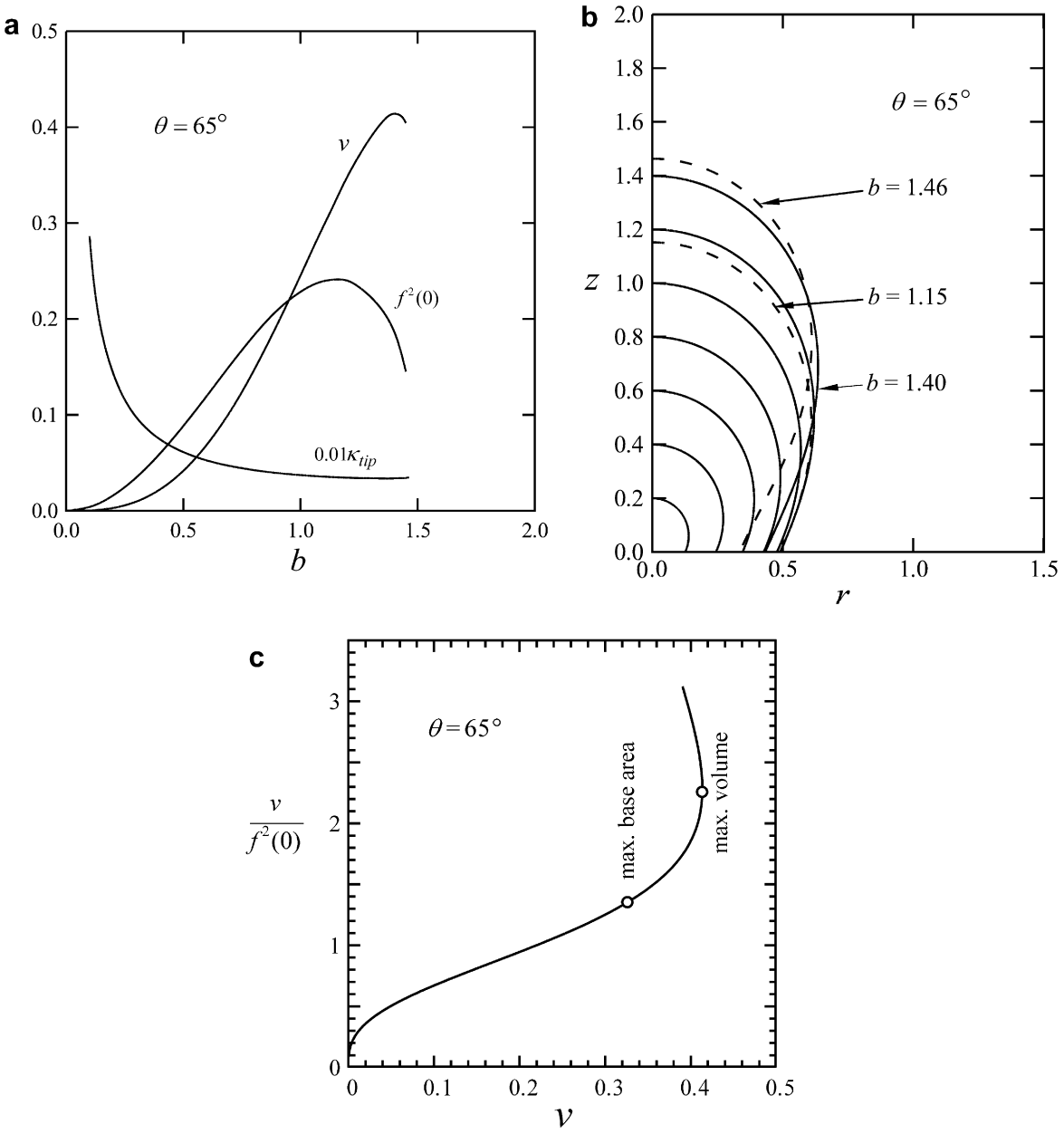

Fig. 4. (a) Bubble volume, base area, and tip curvature as functions of b for solution mode 1. (b) Bubble shapes at various b for solution mode 1. (c) The volume to base area ratio $v/f^2(0)$ versus the volume.

through the bubble surface. The first term is the mass injection directly from the porous surface on the bubble base. Hence, the bubble volume at the next time step can be estimated from

$$v(\tau+\Delta\tau) = v(\tau) + \left(\frac{dv(\tau)}{d\tau}\right)\Delta\tau \tag{23}$$

once the growing rate of the bubble $(dv/d\tau)$ is obtained from Eq. (22a), where $\Delta\tau$ is the time step employed in the numerical simulation.

In the present study, the corresponding bubble height b and tip curvature κ_{tip} are obtained from Fig. 4(a) for a given bubble volume v. Based on the two parameters, the bubble shape $r = f(z)$ is determined with the geometry method [23]. Fig. 6 illustrates the movement of the bubble shape from τ to $\tau + \Delta\tau$. The white dots are the solution of the bubble shape produced by the geometry method. For simplicity, the migrating velocity of the bubble surface is assumed normal to the bubble surface at the time $\tau + \Delta\tau$, i.e.

$$r = f(z, \tau+\Delta\tau) \tag{24}$$

Hence, the arrow from point B to point A as illustrated in Fig. 6 is defined as the displacement of point A during the time interval $[\tau, \tau+\Delta\tau]$ where the arrow is normal to the bubble surface (24) at point A. To take the bubble dilation effect into account, the velocity speed at point A is estimated from

$$v_A = \frac{\overline{BA}}{\Delta\tau}\sqrt{\frac{f(z_B)\Delta a_0}{f(z_A)\Delta a_1}} \tag{25}$$

where $\overline{BA}$ is the distance between points A and B, and z_A and z_B denote the altitude coordinate of point A and B, respectively. The lengths Δa_0 and Δa_1 are defined in Fig. 6. The migration velocity of the bubble surface then is interpolated from the velocities at the white points.

Finally, the associated boundary conditions on the other four boundaries are defined by

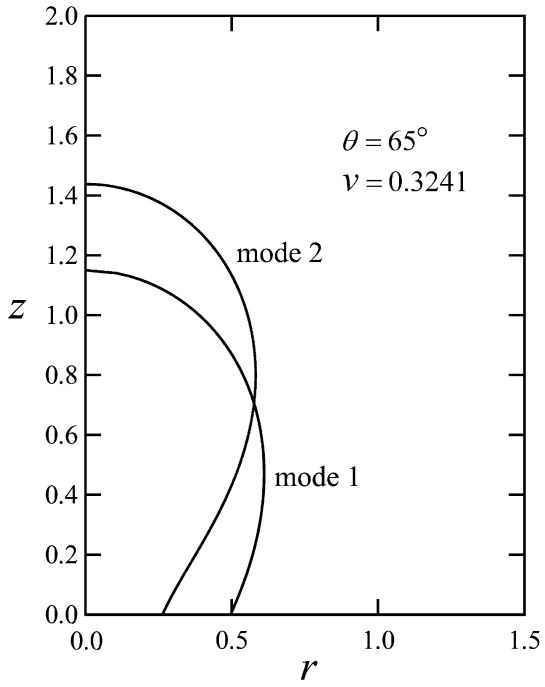

Fig. 5. Bubble shapes for solution modes 1 and 2 having the same volume $v = 0.3241$.

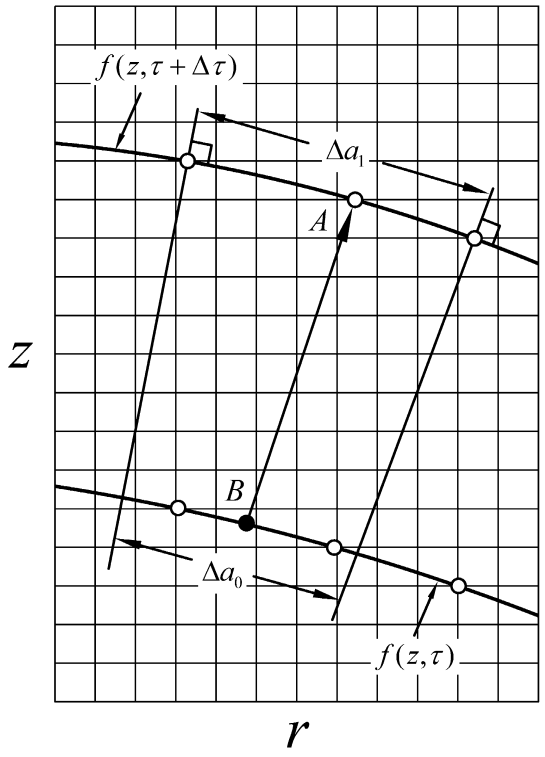

Fig. 6. Estimation of expansion velocity of the bubble surface.

$$\partial u(z,0,\tau)/\partial r = 0, \quad v(z,0,\tau) = 0, \quad \partial\phi(z,0,\tau)/\partial r = 0 \tag{26a}$$

$$\partial u(z,r_0,\tau)/\partial r = 0, \quad v(z,r_0,\tau) = 0, \quad \partial\phi(z,r_0,\tau)/\partial r = 0 \tag{26b}$$

$$u(0,r,\tau) = 0, \quad v(0,r,\tau) = 0, \quad \partial\phi(0,r,\tau)/\partial z = -q \tag{26c}$$

$$\partial u(z_{\max},r,\tau)/\partial z = 0, \quad v(z_{\max},r,\tau) = 0, \quad \phi(z_{\max},r,\tau) = 0 \tag{26d}$$

where the computational domain is truncated at $z = z_{\max}$. Note also that the boundary condition (26a) at the symmetric axis is valid only for $b \leqslant z \leqslant z_{\max}$, while Eq. (26c) is applied only in the region of $f(0) \leqslant r \leqslant r_0$.

3. Result and discussion

Numerical simulation is performed for the contact angle $\theta = 65°$ as mentioned earlier. The system temperature is 25 °C at standard atmospheric pressure ($P_g = 101.3$ kPa). The reference velocity is assigned as $U_c = D_l/L$ such that $Pe_c = 1$. The thermophysical properties used in the computation are

$$\begin{aligned} &\rho_l = 997.0\ \text{kg/m}^3, \quad \mu_l = 0.0008998\ \text{N s/m}^2 \\ &\rho_g = 1.812\ \text{kg/m}^3, \quad \gamma = 0.0720\ \text{N/m}, \\ &H = 68.03\ \text{kPa/(kg/m}^3), \quad D_l = 1.92\times10^{-9}\ \text{m}^2/\text{s} \end{aligned} \tag{27}$$

The corresponding dimensionless parameters are

$$\Theta = 1.217, \quad \Omega = 0.0002617, \quad Re_c = \frac{\rho_l D_l}{\mu_l} = Sc^{-1} = 0.002127 \tag{28}$$

The following quantities will be needed when the dimensionless variables are converted into dimensional quantities

$$\begin{aligned} &g = 9.806\ \text{m/s}^2, \quad L = 2.716\ \text{mm}, \quad U_c = 0.7069\times10^{-6}\ \text{m/s}, \\ &C_{ref} = 1.489\ \text{kg/m}^3, \quad t_c = 3842\ \text{s}, \quad Q_c = 1.053\times10^{-6}\ \text{kg/m}^2\text{s} \end{aligned} \tag{29}$$

In the present study, the weighting function scheme [25] along with the NAPPLE algorithm [26,27] is employed to solve the governing Eqs. (5)–(8) with the associated boundary conditions (20), (22), (25), and (26). The solution procedure starts with a given seed bubble of $v = 0.004401$ ($b = 0.23$) under the initial condition

$$u(z,r,0) = 0, \quad v(z,r,0) = 0, \quad \phi(z,r,0) = 0 \tag{30}$$

The computational domain is truncated at $z_{\max} = 5$. For simplicity, the pressure level is defined by $\hat{p}(z_{\max},r,\tau) = 0$. After some preliminary grid tests, it is found that the numerical solution for the diffusion Eq. (8) is not sensitive to the grid mesh. Hence, a uniform Cartesian grid system $\Delta z = \Delta r = 0.01$ under a uniform time step $\Delta\tau = 0.01$ is employed for all of the computations in the present study.

Fig. 7 shows the evolution of the resulting bubble shape for the case of $r_0 = 3$ and $q = 10$. The velocity on the surface of the seed bubble is zero, and thus $\tau = 0.01$ shares the same bubble profile with $\tau = 0$ as depicted in Fig. 7. In the present case the bubble shrinks at the very beginning of the diffusion process and subsequently grows to the maximum base area and then detaches from the porous surface at $\tau = 0.1412$ with a volume of $v = 0.3241$. At this particular moment, both volume and height of the bubble could be still increasing while the base area of the bubble starts to shrink (see Fig. 4(a)). The solid curves in Fig. 8 show the corresponding concentration distribution at this moment. Fig. 8 shows that the concentration on the liquid side of the bubble surface is essentially unity because the surface tension effect is negligibly small ($\Omega \ll 1$). The mass (carbon dioxide) flux enters the bubble from the lower part (below the iso-concentration curve for $\phi = 1$) while leaves on the upper part. The maximum concentration $\phi = 4.38$ occurs at $(z,r) = (0,1)$. Use of $z_{\max} = 5$ seems to be adequate for the present study.

Bubble detachment from a solid surface is a very complicated fluid flow problem. When the bubble lifts off from the porous surface, the bubble might entrain in its wake of high carbon dioxide concentration. In the present work, this effect is neglected for simplicity. Instead, a fictional concentration with a "seed" bubble represented by the dashed lines in Fig. 8 is employed as the "initial" condition for the growth period of the second bubble. The fictional concentration is defined such that the liquid volume below each iso-concentration surfaces (i.e. $\phi = 0.2, 0.5, \ldots$, etc.) is identical to

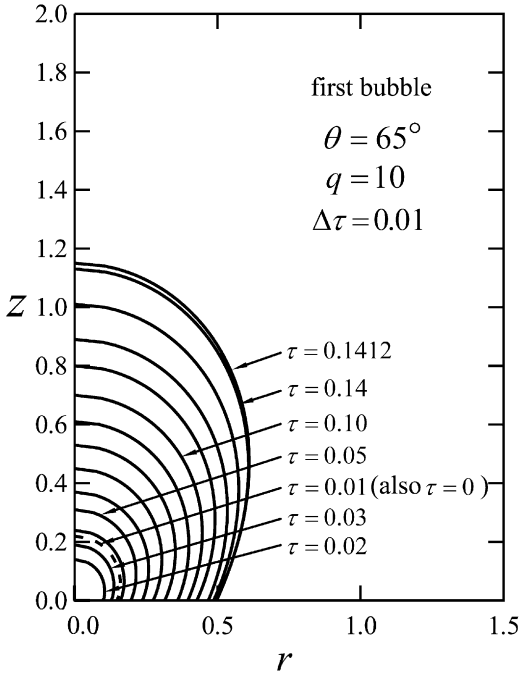

Fig. 7. Expansion of the first bubble for $q = 10$ and $r_0 = 3$.

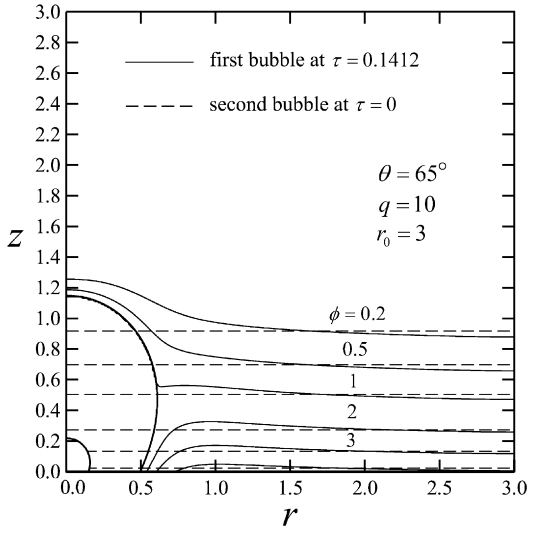

Fig. 8. Comparison of the concentration just before the detachment of the first bubble and the estimated "initial" concentration for the growth period of the second bubble.

the counterpart of the solid curves revealed in Fig. 8. The numerical procedure is repeated for 20 bubbles in the present work. Similar definition of "initial" concentration is employed for each of the other 18 bubbles. Bubble shrinkage is found to occur only at the very beginning of the growth period of the first bubble due to the assumed zero concentration in the environment liquid. Fig. 9 shows the concentration just before the detachment of the 20th bubble. The maximum concentration occurs at $\phi(0, 0.672) = 8.42$. This implies that bubble nucleation might take place on the porous surface [28] in the vicinity of the main bubble similar to that observed by Nam et al. in their experiment [10]. Nevertheless, homogeneous nucleation in the liquid does not seem possible. It requires a supersaturation of $1100 \leqslant \phi \leqslant 1700$ for carbonated beverage as reported by Wilt [28].

Fig. 10(a) shows the bubble growth time τ_n required for the nth bubble under $(\theta, q) = (65°, 10)$ and various values of r_0. As expected, the growth time deceases as the bubble number increases due to the increasing concentration in the environment liquid. For instance, the growth times decrease from $\tau_1 = 0.1489$ to $\tau_{20} = 0.01558$ when $r_0 = 1$; from $\tau_1 = 0.1475$ to $\tau_{20} = 0.007549$ when $r_0 = 2$; and from $\tau_1 = 0.1412$ to $\tau_{20} = 0.007139$ when $r_0 = 3$. The first bubble always takes a very long time to grow as compared to the second bubble. The radius of the diffusion domain for a nucleation site r_0 seems to have only little influence on the growth time of the first bubble. Moreover, it shows essentially no influence on the growth time for $n \geqslant 8$ when r_0 is large ($r_0 \geqslant 2$). The growth time of bubbles under the parameters $(\theta, r_0) = (65°, 2)$ for various mass fluxes is shown in Fig. 10(b). For $q = 10$, 50, 100, the growth time of the first bubble is $\tau_1 = 0.1475$, 0.04262, 0.03073, respectively, while the growth time of the 20th bubble is $\tau_{20} = 0.007549$, 0.002163, 0.001820, respectively. Increasing the mass flux is seen to decrease the required growth time.

In the present problem, both diffusion coefficient D_l and fluid flow due to bubble growth are very small. Hence, bubble detachment from the porous surface becomes the major means of mass transport (see Fig. 9 for instance). The efficiency of mass transport by bubble detachment during the growth period of the 20th bubble is defined as

$$\eta = \frac{\Delta v \Theta}{\tau_{20} r_0^2 q} \tag{31}$$

where Δv is the volume difference between the maximum bubble ($v = 0.3241$) and the "seed" bubble ($v = 0.004401$). The denominator of Eq. (31) represents the total mass injection from the porous surface during the growth period of the 20th bubble while the numerator denotes the mass increase inside the bubble during the same time interval. The efficiency under the parameters $(\theta, q) = (65°, 10)$ is 2.421, 1.249, and 0.5871 for $r_0 = 1$, 2, and 3, respectively. At $(\theta, r_0) = (65°, 2)$ the efficiency is 1.249, 0.8720, and 0.5182 for $q = 10$, 50, and 100, respectively.

Finally, the computations are repeated for $\theta = 30°$ to investigate the contact angle effect. Fig. 11 reveals the bubble shapes at various bubble heights. The solution procedure starts with a given seed bubble of $v = 0.00025$ ($b = 0.1$). The bubble is assumed to detach when the maximum base area is reached at $v = 0.02502$

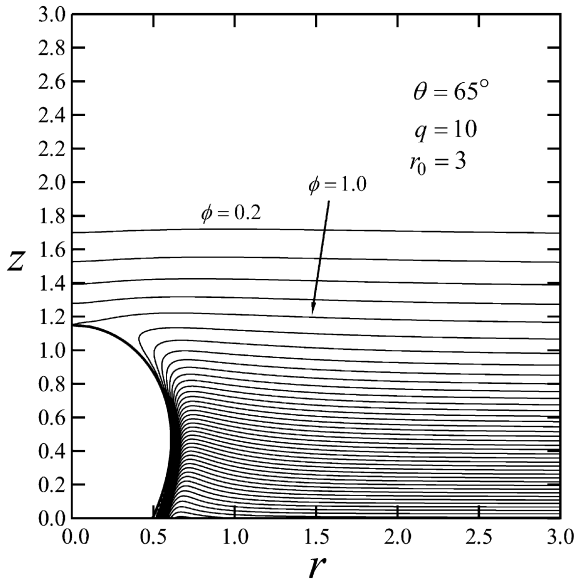

Fig. 9. Concentration just before the detachment the 20th bubble.

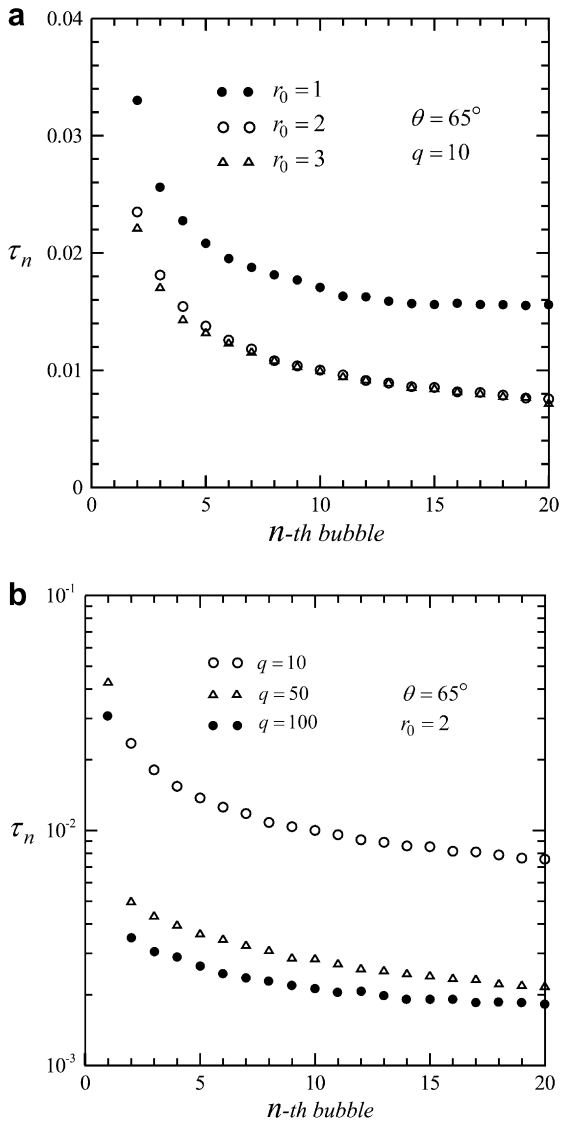

Fig. 10. (a) Influence of r_0 on the growth time of the nth bubble at $q = 10$ and $\theta = 65°$. (b) Influence of q on the growth time of the nth bubble at $r_0 = 2$ and $\theta = 65°$.

($b = 0.524$). The resulting bubble growth time is shown in Fig. 12 under various parameters of r_0 and q. The growth time of the first bubble in the case of $(r_0, q) = (2, 10)$ is $\tau_1 = 0.06636$ which is not plotted in the figure. The efficiency under the parameters $(\theta, q) = (30°, 10)$ is 0.6280, 0.1570, and 0.06978 for $r_0 = 1$, 2, and 3, while that under $(\theta, r_0) = (30°, 2)$ is 0.1570, 0.04433, and 0.02355 for $q = 10$, 50, and 100. The low mass transport efficiency found in the case of $\theta = 30°$ might be attributed to the small bubble surface area. This indicates that hydrophobic surface produces large bubble and thus gives rise to better efficiency for dissolved gas removal.

4. Conclusion

Growth and detachment of carbon dioxide bubbles on a horizontal porous surface with a uniform mass injection is investigated in the paper. Based on the cases studied in the present work, the following conclusions are drawn:

(a) The bubble volume is determined by the mass diffusion in the problem. Evolution of bubble shape can be obtained by solving the Young–Laplace equation once the bubble volume is known.

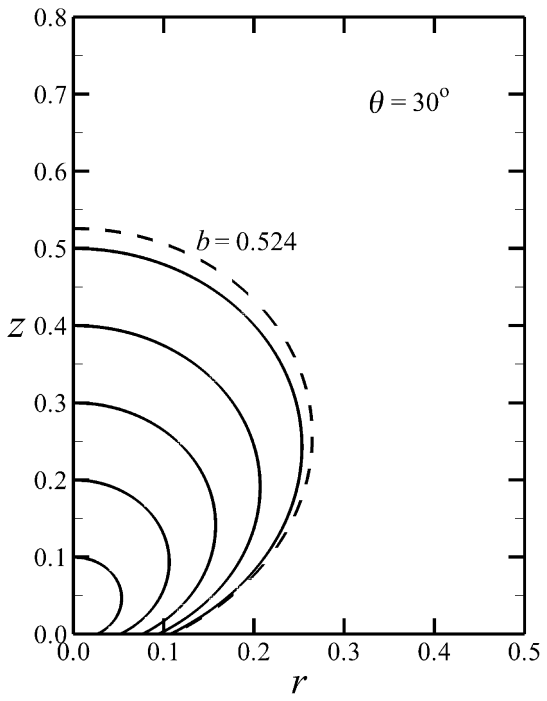

Fig. 11. Bubble shapes at various b for solution mode 1 under $\theta = 30°$.

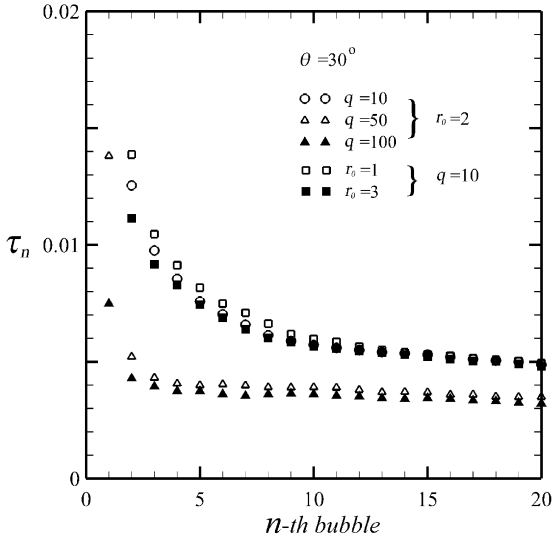

Fig. 12. Growth time of the nth bubble at various q and r_0 under $\theta = 30°$.

(b) Multiple solutions modes are found for a given volume.
(c) It is postulated that the bubble grows with a monotonically increasing base area until the maximum value is reached according to the fundamental solution mode. After that, the bubble jumps toward the secondary solution mode at a constant volume, and then detaches from the surface.
(d) Hydrophobic surface produces large bubble and thus gives rise to better efficiency for dissolved gas removal.

Acknowledgments

The authors express their appreciation to Mr. You-Ruei Liou for his preparation of Figs. 11 and 12. This work is supported by National Science Council of Taiwan through the contract NSC 95-2218-E-007-002.

References

[1] H.N. Oguz, A. Prosperetti, Dynamics of bubble growth and detachment from a needle, J. Fluid Mech. 257 (1993) 111–145.
[2] I. Kim, Y. Kamotani, S. Ostrach, Modeling bubble and drop formation in flowing liquids in microgravity, AIChE J. 40 (1994) 19–28.
[3] N. Sonoyama, M. Iguchi, Bubble formation and detachment on nonwetted surface, Metall. Mater. Trans. B 33B (2002) 155–162.
[4] G. Duhar, C. Colin, A predictive model for the detachment of bubbles injected in a viscous shear flow with small inertial effects, Phys. Fluids 16 (2004) L31–L34.
[5] G. Duhar, C. Colin, Dynamics of bubble growth and detachment in a viscous shear flow, Phys. Fluids 18 (2006). 077101-1-13.
[6] M. Martin, F.J. Montes, M.A. Galan, Numerical calculation of shapes and detachment times of bubbles generated from a sieve plane, Chem. Eng. Sci. 61 (2006) 363–369.
[7] L.Z. Zeng, J.F. Klausner, R. Mei, A unified model for the prediction of bubble detachment diameters in boiling systems – I. Pool boiling, Int. J. Heat Mass Transfer 36 (1993) 2261–2270.
[8] C.W.M. van der Geld, Prediction of dynamic contact angle histories of a bubble growing at a wall, Int. J. Heat Fluid Flow 25 (2004) 74–80.
[9] Y. Chen, M. Groll, Dynamics and shape of bubbles on heating surfaces: a simulation study, Int. J. Heat Mass Transfer 49 (2006) 1115–1128.
[10] Y. Nam, G. Warrier, J. Wu, Y.S. Ju, Single bubble dynamics on a hydrophobic surface, in: The ASME-JSME 2007 Thermal Engineering and Summer Heat Transfer Conference, Vancouver, Canada.
[11] C.G.J. Bisperink, A. Prins, Bubble growth in carbonated liquids, Colloids Surf. A Physicochem. Eng. Aspects 85 (1994) 237–253.
[12] S.F. Jones, G.M. Evans, K.P. Galvin, Bubble nucleation from gas cavities – a review, Adv. Colloid Interface Sci. 80 (1999) 27–50.
[13] S.F. Jones, G.M. Evans, K.P. Galvin, The cycle of bubble production from a gas cavity in a supersaturated solution, Adv. Colloid Interface Sci. 80 (1999) 51–84.
[14] S. Uzel, M.A. Chappell, S.J. Payne, Modeling the cycles of growth and detachment of bubbles in carbonated beverages, J. Phys. Chem. B 110 (2006) 7579–7586.
[15] E. Pitts, The stability of pendent liquid drops. Part 2. Axial symmetry, J. Fluid Mech. 63 (1961) 487–508.
[16] A.K. Chesters, An analytical solution for the profile and volume of a small drop or bubble symmetrical about a vertical axis, J. Fluid Mech. 81 (1977) 609–624.
[17] A.K. Chesters, Modes of bubble growth in the slow-formation regime of nucleate pool boiling, Int. J. Multiphase Flow 4 (1978) 279–302.
[18] C.W.M. van der Geld, Bubble detachment criteria: some criticism of Das Abreissen von Dampfblasen an festen Heizflachen, Int. J. Heat Mass Transfer 39 (1996) 653–657.
[19] J. Mitrovic, Bubble detachment criteria, Int. J. Heat Mass Transfer 40 (1997) 209–211.
[20] G.Q. Lu, C.Y. Wang, Electrochemical and flow characterization of a direct methanol fuel cell, J. Power Sources 134 (2004) 33–40.
[21] S.F. Kistler, Hydrodynamics of wetting, in: J.C. Berg (Ed.), Wettability, Marcel Dekker, New York, 1993, pp. 311–429.
[22] T. Sarpkaya, Vorticity, free surface and surfactants, Annu. Rev. Fluid Mech. 28 (1996) 83–128.
[23] S.L. Lee, H.D. Lee, Evolution of liquid meniscus shape in a capillary tube, ASME J. Fluids Eng. 129 (2007) 957–965.
[24] P.G.T. Fogg, W. Gerrard, Solubility of Gasses in Liquids, Wiley, Chichester, England, 1991. pp. 24, 242, 243.
[25] S.L. Lee, Weighting function scheme and its application on multidimensional conservation equations, Int. J. Heat Mass transfer 32 (1989) 2065–2073.
[26] S.L. Lee, R.Y. Tzong, Artificial pressure for pressure-linked equation, Int. J. Heat Mass Transfer 35 (1992) 2705–2716.
[27] S.L. Lee, D.W. Lin, Transient conjugate heat transfer on a naturally cooled body of arbitrary shape, Int. J. Heat Mass Transfer 40 (1997) 2133–2145.
[28] P.M. Wilt, Nucleation rates and bubble stability in water–carbon dioxide solutions, J. Colloid Interface Sci. 112 (1986) 530–538.